Scripta Materialia 255 (2025) 116403

Contents lists available at ScienceDirect

Scripta Materialia

journal homepage: www.journals.elsevier.com/scripta-materialia

A self-consistent void-based rationale for hydrogen embrittlement

Haiyang Yu [a], Jianying He [b], David Didier Morin [b], Michael Ortiz [c], Zhiliang Zhang [b,*]

[a] Division of Applied Mechanics, Department of Materials Science and Engineering, Uppsala University, Uppsala SE-75121, Sweden
[b] Department of Structural Engineering, Norwegian University of Science and Technology (NTNU), Trondheim 7491, Norway
[c] Graduate Aerospace Laboratories, California Institute of Technology, 1200 E. California Blvd., Pasadena, CA 91125, USA

ARTICLE INFO

Keywords:
Hydrogen embrittlement
Microvoid process
Ductile-to-brittle transition

ABSTRACT

Solely based on the failure process of metallic materials containing voids, we propose a straightforward rationale for a self-consistent void-based hydrogen embrittlement (CVHE) predictive framework that effectively captures ductile failure, hydrogen-induced loss of ductility, and most importantly, the ductile-to-brittle transition. While the coupling effect of homogenously distributed secondary voids is well-documented, the rigor of our approach lies in the precise definition of an array of equally sized and spaced secondary voids nucleated aligning with the hydrogen embrittlement mechanisms HEDE, HELP and HESIV, in the ligament between primary voids. The CVHE model can quantitatively predict the full range of embrittlement; it naturally reveals the brittle inter-ligament decohesion associated with an intrinsic lower bound of ductility, when the secondary voids are sufficiently small. Counterintuitively, our results show that ductility reduction accelerates with a decrease in the secondary void volume fraction, and that smaller voids lead to greater embrittlement.

Hydrogen embrittlement (HE) poses a significant safety threat to engineering structures used in green hydrogen applications, such as hydrogen transport pipelines, cryogenic hydrogen storage tanks, and steel liners in hydrogen storage caverns [42]. Predictive models for HE are crucial for structural integrity assessment and lifetime forecasting of these structures. Void-based modelling approaches possess a high potential to link the model parameters to the microstructures of materials and ensure engineering transferability. An example is the Gurson–Tvergaard–Needleman (GTN) model [16,3,30] which has achieved substantial success in predicting ductile failure of metals [5–7,25]. This model captures the essence of ductile fracture through the microvoid failure process by employing a void volume fraction parameter to characterize the nucleation, growth and coalescence of voids. An extended version of the GTN model is called the Complete Gurson Model (CGM) [45]. The GTN model uses a negotiable critical void volume fraction to depict void coalescence. In contrast, the CGM provides an additional localized deformation mode [38] to physically capture void coalescence.

Microvoid process is not an exclusive signature of ductile fracture. Small voids have been observed in a variety of materials undergoing HE, for example, in iron [22], steel [26] and nickel alloys [18,36]. Often, these voids became much smaller in the presence of hydrogen and were only distinguishable at high resolution, decorating the fracture surfaces that appeared smooth and featureless when observed at lower magnification [33,16,17,2]. Hydrogen-voids interactions have been extensively studied using a representative volume element, or unit cell, containing a void [2,19,44], highlighting the potential of Gurson models in the prediction of HE. In 2001, Nagumo et al. [29] applied the GTN model to simulate the R curves of non-charged and hydrogen-charged specimens, and found that a larger void nucleation parameter was needed in the case with hydrogen, consistent with the hydrogen-enhanced strain-induced vacancy (HESIV) mechanism [35]. In 2019, Yu et al. [17] proposed a hydrogen-informed GTN (H-GTN) model, where void growth rate scales with hydrogen concentration as calibrated from unit cell analyses. Based on the GTN model, hydrogen enhanced void nucleation was introduced [17] and a non-local version [1] was recently proposed. Based on the CGM, hydrogen enhanced void nucleation and growth were implemented, yielding a H-CGM model [9]. Further, a so-called H-CGM+ model was established to combine hydrogen induced decohesion into the H-CGM model [24]. The studies indicated that the influence of hydrogen on void growth rate might be negligible, while the focus should be placed on hydrogen enhanced void nucleation. Void nucleation can be triggered by a number of microstructural features [33], for example, through the decohesion of particle–matrix interface in a stress-controlled manner, or by dislocation entanglement and vacancy condensation, which is strain-controlled.

* Corresponding author.
E-mail address: zhiliang.zhang@ntnu.no (Z. Zhang).

https://doi.org/10.1016/j.scriptamat.2024.116403
Received 11 September 2024; Accepted 29 September 2024
Available online 4 October 2024

According to the HESIV mechanism, hydrogen facilitates the generation of vacancies in plastically deformed zones and promotes the nucleation of voids [28]. The hydrogen-enhanced localized plasticity (HELP) mechanism suggests that hydrogen accelerates void growth [2] and facilitates strain-controlled void nucleation. The hydrogen enhanced decohesion (HEDE) mechanism suggests that hydrogen could promote stress-controlled void nucleation at inclusions.

In classical void-based ductile failure theory, larger void sizes (and higher void volume fractions) are associated with reduced ductility, suggesting that larger voids are needed to capture the hydrogen-induced reduction in ductility. However, smaller voids are essential to capture the hydrogen-induced brittle fracture patterns. This apparent contradiction has persisted since the introduction of hydrogen-informed Gurson models.

In this study, we propose a consistent void-based rationale for HE that resolves this paradox. Our approach is based on a plain mechanistic interpretation of the ductile-to-brittle fracture transition, which we define as a shift from an extended fracture process zone to a highly confined one, as depicted in Fig. 1(a). The extended process zone aligns with the classical void growth and coalescence mechanism, while the confined fracture process zone, characterized by the presence of very small voids, is supported by substantial experimental evidence as mentioned earlier. These small voids can emerge through various sub-micron processes, and their contribution to failure can reasonably be scaled by their overall void volume fraction, smearing their effect across the fracture process zone, as done in the classical Gurson model [3].

So far, we have attributed ductile and hydrogen-induced fractures to two distinct types of fracture process zones: one containing large voids in the absence of hydrogen, and the other characterized by much smaller voids in the presence of hydrogen. For clarity, we classify these voids into primary and secondary types. Consistently, both void types are proposed to be smeared within their respective fracture process zones when assessing their impact on failure. Fig. 1(b) illustrates a unit cell model with a central primary void and a confined fracture process zone, where smaller secondary voids form in the central ligament where stress and strain are concentrated. Given the current micromechanical model,

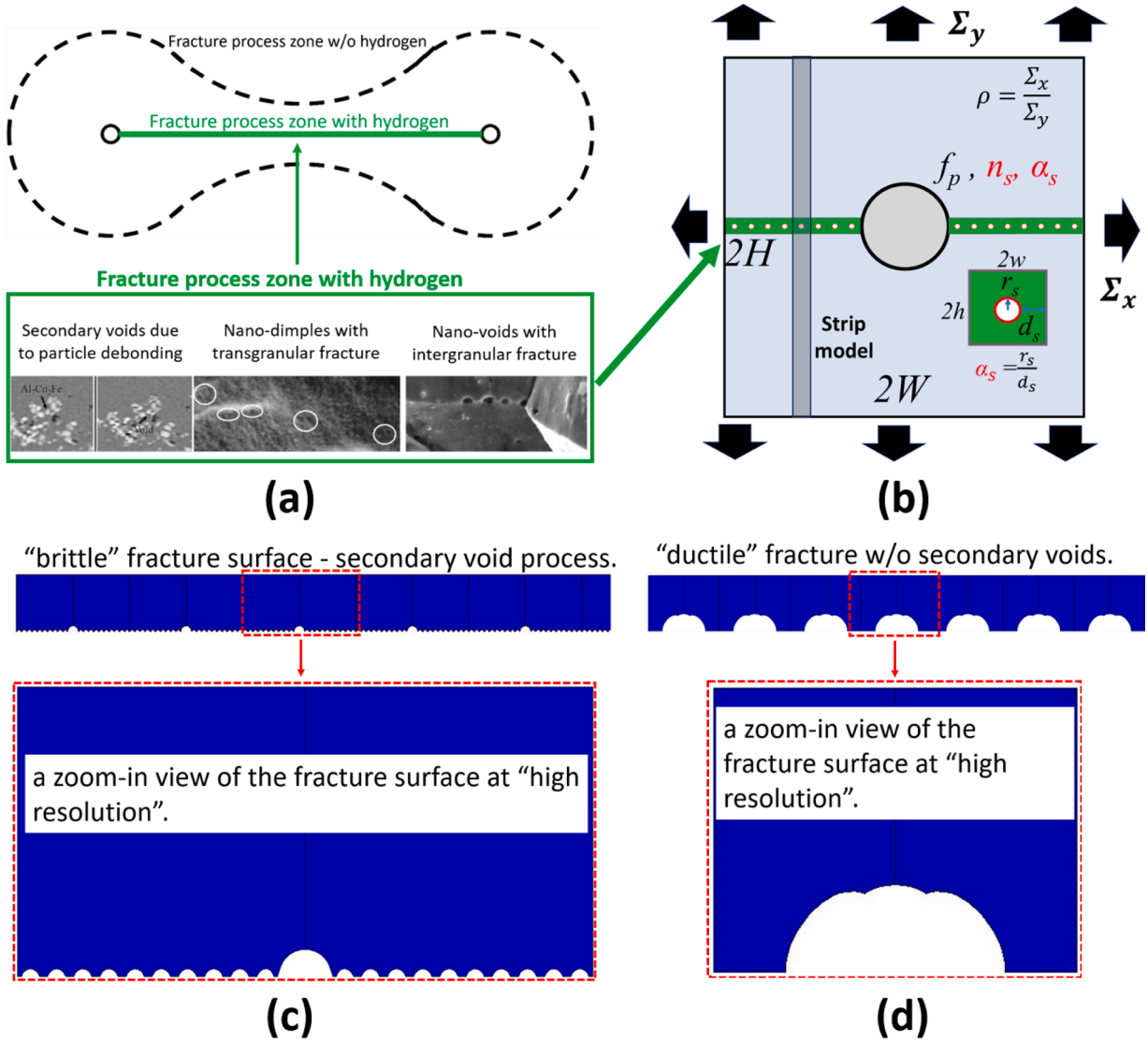

Fig. 1. (a) A schematic illustration of the consistent void-based rationale for HE. Hydrogen leads to a confined fracture process zone populated with small secondary voids formed due to particle debonding [41], vacancy condensation [31] and grain boundary voiding [21]. (b) A self-consistent void-based HE (CVHE) model representing the fracture process zone with hydrogen. The size of the primary void is characterised by the initial primary void volume fraction f_p; diameter-to-space ratio, $\alpha_s = r_s/d_s$, is defined to describe the size of the secondary voids in relation to their ligament. The number of secondary voids $2n_s$. (c) The quarter model is mirrored and patterned during postprocessing to produce an image of the fracture surface. The fracture surface appears "brittle" with extremely small dimples, in contrast to (d) the ductile fracture surface, which has obviously larger dimples.

a straightforward way to represent the smeared-secondary voids concept is to populate a uniform array of secondary voids within the confined fracture process zone. This representation introduces two parameters: the initial void diameter-to-spacing ratio (α_s) and the number of secondary voids (n_s) along half of the ligament. By fixing α_s and varying n_s, we can explore the effect of secondary void size while keeping the total initial ligament length constant. For a given primary void size and secondary void diameter-to-spacing ratio, the total volume fraction of secondary voids decreases as n_s increases, approaching zero when n_s is sufficiently large.

This model is expected to have broad applicability, supported by experimental evidence of small secondary voids observed in various alloys. However, it is important to acknowledge that no model can be universally applicable due to the complex nature of HE. For instance, this model does not account for fractures associated with phase transformation. Therefore, the presence of secondary voids must be experimentally confirmed before applying the model to any specific material.

It must also be acknowledged that the concept of secondary void-mediated failure is not new. Research in this area can be categorized into two main types. The first type explicitly models only the primary void, while treating secondary voids implicitly by modeling the matrix as a porous material, characterized by a secondary void volume fraction [31–33,12]. The second type explicitly models both primary and secondary voids, allowing for an analysis of how the distribution of secondary voids influences failure [10,36,37,39]. The novelty of the current work lies in the precise definition of an array of secondary voids in such a way that whole embrittlement range, including ductile failure without hydrogen, can be achieved by regulating the two parameters of the secondary voids, α_s and n_s.

We used plane strain condition and a constant biaxial stress ratio to demonstrate the predictability of the CVHE model. In the present demonstration, it is assumed that the secondary voids are nucleated simultaneously with the primary voids. In a practical application, an incubation process for the nucleation of the secondary voids is often needed. The incubation history can be conveniently added to the model. Following the method proposed by Faleskog et al. [13], the boundaries of the unit cell were kept straight during loading, and the displacements of the boundaries were controlled via a UMPC subroutine in the commercial finite element software Abaqus. The J2 flow theory with isotropic hardening was used to describe the cell matrix material [43].

The failure of the unit cell containing only a primary void is correlated with plastic instability in the ligament between the primary voids, i.e. void coalescence [20]. When both n_s and α_s are large, plastic instability will be triggered in the ligaments of the array of secondary voids, as shown in Fig. 1(b), and the failure of the unit cell is correlated with the coalescence of these secondary voids, which occurs much earlier than that of the primary voids. By postprocessing the quarter cell model at failure, as illustrated in Fig. 1(c), a "fracture surface" was visualized. Due to the small size of both the secondary voids and the primary void, the fracture surface appeared "flat" at low magnification, in contrast to the clearly dimpled fracture surface generated by the failure of a single void-containing cell, as shown in Fig. 1(d). The presence of secondary voids appears to "embrittle" the unit cell.

The “embrittlement” effect of secondary voids is also illustrated by the stress-strain plots in Fig. 2. Fig. 2(a) shows that for given primary void size and loading condition, which determine the upper bound ductility, the extent of embrittlement can be regulated by varying the α_s and n_s. Fig. 2(b) reveals a more brittle failure behavior as the α_s ratio increases, i.e. when the secondary voids become larger relative to their ligament.

So far, the CVHE model has successfully captured the full range of ductile-to-brittle transition. This model is consistently based on the void-mediated failure process and can be conveniently linked to the HEDE, HESIV and HELP mechanisms. Even more intriguing in Fig. 2(b) is that the ductility of the unit cell continues to decrease as the number of secondary voids increases. For both cases with $n_s = 50$, failure has become quite brittle, effectively capturing the brittle separation of the ligament between primary voids. To explore whether this trend continues as n_s increases further and to find a rationale, we simulated a series of “clean” unit cells, by setting $f_p = 0$, i.e. removing the primary void and keeping only the array of secondary voids, and increased n_s up to 500.

Fig. 3(a) shows that the ductility of the unit cell decreases consistently with n_s given a constant α_s ratio, even though the total void volume fraction of these voids also decreases. The loading curves before failure for the cases $n_s = 50$ and $n_s = 500$ seem to overlap, indicating that further increases in n_s are unlikely to alter the failure behaviour significantly. This has practical significance. When the number of secondary voids is sufficiently large, and when the size of the voids and the associated plasticity zone becomes small enough, the ductility converges at a small value, and the fracture surface appears flat—this is "embrittlement." The HESIV mechanism suggests possible presence of nanovoids in a region with intense plasticity (e.g., the ligament between primary voids). Our study provides a rationale for the embrittlement due to that mechanism. Moreover, the fact that the failure strain converges enables a quantitative prediction.

Fracture strength and ductility are captured by the CVHE model as the maximum principal stress and equivalent strain at the onset of void

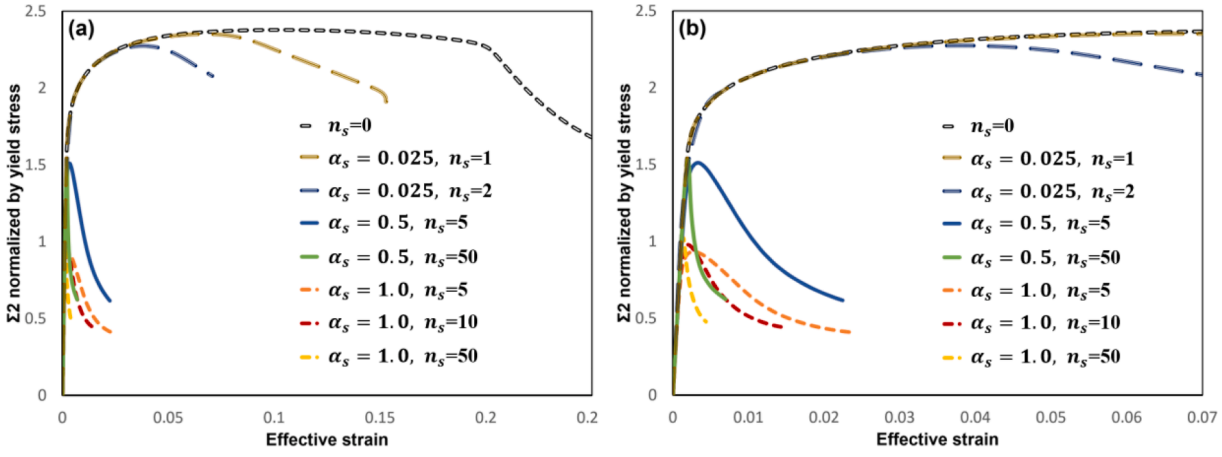

Fig. 2. The stress-strain curves of the unit cells with different α_s ratios and number of secondary voids n_s, under the same biaxial stress ratio $\rho = 0.4$, which approximates a stress triaxiality of 1.0. (b) is a zoomed-in view of (a). Cases with secondary voids exhibit lower strength and significantly reduced ductility compared to the case without secondary voids ($n_s = 0$).

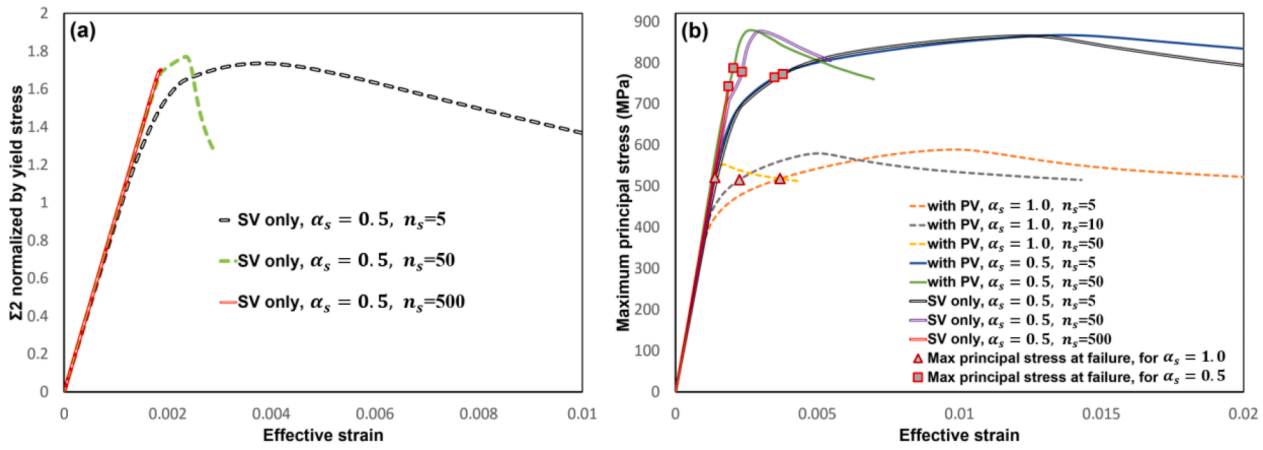

Fig. 3. (a) Stress-strain curves of unit cells under the same biaxial stress ratio $\rho = 0.4$. Ductility keeps decreasing when the number of secondary voids increases. (b) Maximum principal stress curves, evaluated based on the definition in Thomason's plastic limit-load theory. The failure initiation point was determined following the practice of Koplik and Needleman [20] and marked on each curve. In both figures, "SV only" refers to unit cells containing only secondary voids, "with PV" refers to cells containing both a primary void and secondary voids.

coalescence [20], as shown in Fig. 3(a). Maximum principal stress history curves are plotted in Fig. 3(b), as detailed in the figure caption, with the maximum principal stress at the point of failure initiation marked. It can be observed that the critical maximum principal stress remains almost constant, with reasonably small variation, for the same α_s value across different n_s values. We may conclude that α_s determines the fracture strength. Considering that both the plastic deformation and void geometry changes before failure are limited, the nearly constant fracture strength is in line with the Thomason's plastic limit-load theory [5], which suggests that the threshold stress for plastic instability depends on void size/space ratio.

We further utilize a strip model, considering a thin slice specimen with a void at its center, as shown in Fig. 4(a). This model reasonably represents the damage associated to a single secondary void. At failure, the strip model can be divided into a plastic instability zone, a transition zone, and a homogenous zone, from the center of the model to its upper boundary, as illustrated in Fig. 4(a). This division is verified in Fig. 4(b) by plotting the variation of equivalent plastic strain at failure.

Given an α_s of the secondary voids, the resistance of the ligament to failure, fracture strength, is nearly constant, the tensile stress in the upper zone of the strip model at failure can be approximated, and the strain can be readily calculated. The plastic instability zone size L_p inversely scales with n_s. When the size of the secondary voids is sufficiently small, the failure strain of the strip is approximated as the strain at failure, which gives the lower ductility limit. Detailed derivation and verification of the strip model are presented in Supplementary Materials. This strip model highlights that in the limit case the fracture process zone is extremely confined, which reveals brittle decohesion. Note that the growth of these secondary voids is not a premise for ligament failure, because localized deformation of secondary ligaments can be well triggered by the very high stress concentration to the small secondary voids. According to strain gradient plasticity theory, the growth of voids smaller than a certain size is practically prohibited [12], our model does not conflict with this size effect.

Now we can conclude this work by proposing a self-consistent void-based framework for HE, which we refer to as the CVHE model. To start with, hydrogen enhances the nucleation of secondary, small voids in the ligament between pre-existing primary voids. The secondary voids can stem from the interaction between hydrogen and defects. The CVHE model can account for the whole range of embrittlement, by adjusting the size and number of secondary voids. Ductile failure without hydrogen is retrieved by setting the number of secondary voids to zero, while hydrogen induced brittle failure is captured with a large number of secondary voids. Plasticity-mediated and hydrogen enhanced decohesion and brittle decohesion with negligible plasticity are encapsulated in the model, as localization failure of secondary voids occur significantly earlier than that of primary voids, which results in prominent embrittlement. Specifically, for a constant ratio between secondary void diameter and their spacing, the degree of embrittlement escalates with an increase in the number of secondary voids. When the number

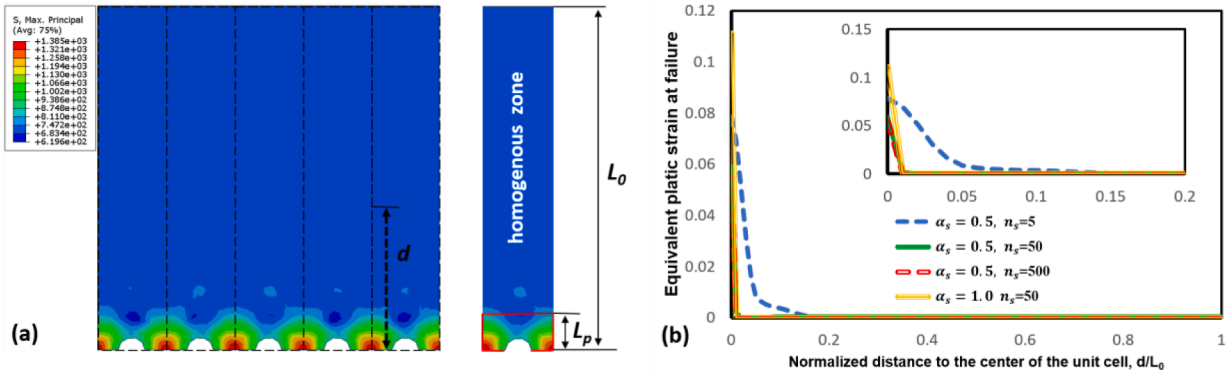

Fig. 4. (a) Illustration of the strip model. The loading pattern of the secondary voids is approximated as a thin strip of material containing a single void at the center. At failure, the void ligament undergoes plastic instability, with intensive plasticity occurring near the voids. Beyond the length of L_p, plasticity diminishes, creating an elasticity or minimal plasticity zone. (b) The variation of equivalent plastic strain from the center of the strip model to the upper boundary.

approaches infinite, the size of localized plastic zone approaches zero, resulting in brittle decohesion of the primary void ligament. Notably, the lower bound ductility in this limit case can be theoretically derived with a strip model.

From another perspective, the CVHE model represents a void sheet mechanism specific to HE, which may ultimately be regarded as a process of localization of damage controlled by microplasticity. A careful analysis based on optimal scaling [4,14,43,44] shows that the effective behaviour of the void sheet takes the form of a cohesive law. The effective cohesive law can be conveniently embedded in large-scale finite-element models at the macroscale [34], as a supplement to existing hydrogen degradation laws. In this direction, exciting further work is undergoing, to develop a CGM-type constitutive equation based on the CVHE concept, which will be integrated into a predictive framework for HE.

CRediT authorship contribution statement

Haiyang Yu: Conceptualization, Formal analysis, Investigation, Methodology, Validation, Writing – original draft, Writing – review & editing. **Jianying He:** Investigation, Methodology, Writing – review & editing. **David Didier Morin:** Methodology, Writing – review & editing. **Michael Ortiz:** Methodology, Writing – review & editing. **Zhiliang Zhang:** Conceptualization, Funding acquisition, Investigation, Methodology, Project administration, Writing – review & editing.

Declaration of competing interest

The authors declare that they have no known competing financial interests or personal relationships that could have appeared to influence the work reported in this paper.

Acknowledgements

ZZ acknowledges the financial support from the Research Council of Norway via the “Safety and Integrity of Hydrogen Transport Pipelines” project (HyLine II, Project No.344377) and “Microstructure-Informed Hydrogen Embrittlement Life Prediction of Nickel-Based Alloys” project (Helife, Project No. 344297). ZZ and HY acknowledge the financial support from Nordic Energy Research, Research Council of Norway (Project No. 347726) and Swedish Energy Agency (P2023-00687) via the “Material and structural integrity assessment for safe Nordic hydrogen transportation infrastructure” project. HY acknowledges the financial support from Swedish Research Council (VR Starting Grant 2023-05055).

Supplementary materials

Supplementary material associated with this article can be found, in the online version, at doi:10.1016/j.scriptamat.2024.116403.

References

[1] D.L. Pinto, A. El Ouazani Tuhami, N. Osipov, Y. Madi, J. Besson, Simulation of hydrogen embrittlement of steel using mixed nonlocal finite elements, Eur. J. Mech. A/Solids 104 (2024) 105116.
[2] D.C. Ahn, P. Sofronis, R.H. Dodds, On hydrogen-induced plastic flow localization during void growth and coalescence, Int. J. Hydrog. Energy 32 (16) (2007) 3734–3742.
[3] T.L. Anderson, T.L. Anderson, Fracture Mechanics: Fundamentals and Applications, CRC Press, 2005.
[4] M.P. Ariza, S. Conti, M. Ortiz, Fractional strain gradient plasticity and ductile fracture of metals, Eur. J. Mech. A/Solids 104 (2024) 105172.
[5] A.A. Benzerga, J.B. Leblond, Ductile fracture by void growth to coalescence, in: H. Aref, E.V.D. Giessen (Eds.), Advances in Applied Mechanics, Elsevier, 2010, pp. 169–305.
[6] S. Bergo, D. Morin, O. Sture Hopperstad, Numerical implementation of a non-local GTN model for explicit FE simulation of ductile damage and fracture, Int. J. Solids Struct. 219-220 (2021) 134–150.
[7] J. Besson, D. Steglich, W. Brocks, Modeling of crack growth in round bars and plane strain specimens, Int. J. Solids Struct. 38 (46) (2001) 8259–8284.
[8] S. Conti, M. Ortiz, Optimal scaling in solids undergoing ductile fracture by crazing, Arch. Ration. Mech. Anal. 219 (2) (2016) 607–636.
[9] R. Depraetere, W. De Waele, S. Hertelé, Fully-coupled continuum damage model for simulation of plasticity dominated hydrogen embrittlement mechanisms, Comput. Mater. Sci. 200 (2021) 110857.
[10] A. Dwivedi, I. Khan, J. Chattopadhyay, On the role of shape and distribution of secondary voids in the mechanism of coalescence, Eng. Fract. Mech. 289 (2023) 109399.
[11] V. Espeseth, D. Morin, J. Faleskog, T. Børvik, O.S. Hopperstad, A numerical study of a size-dependent finite-element based unit cell with primary and secondary voids, J. Mech. Phys. Solids 157 (2021) 104493.
[12] D. Fabrègue, T. Pardoen, A constitutive model for elastoplastic solids containing primary and secondary voids, J. Mech. Phys. Solids 56 (3) (2008) 719–741.
[13] J. Faleskog, X. Gao, C.F. Shih, Cell model for nonlinear fracture analysis – I. Micromechanics calibration, Int. J. Fract. 89 (4) (1998) 355–373.
[14] L. Fokoua, S. Conti, M. Ortiz, Optimal scaling in solids undergoing ductile fracture by void sheet formation, Arch. Ration. Mech. Anal. 212 (1) (2014) 331–357.
[15] L. Fokoua, S. Conti, M. Ortiz, Optimal scaling laws for ductile fracture derived from strain-gradient microplasticity, J. Mech. Phys. Solids 62 (2014) 295–311.
[16] A.L. Gurson, Plastic Flow and Fracture Behavior of Ductile Materials Incorporating Void Nucleation, Growth, and Interaction, Brown University, 1975.
[17] A.E. Halilović, A Fracture Mechanics Approach to Study Hydrogen Embrittlement in High Strength Martensitic Steels, KTH Royal Institute of Technology, 2023.
[18] Z.D. Harris, J.J. Bhattacharyya, J.A. Ronevich, S.R. Agnew, J.T. Burns, The combined effects of hydrogen and aging condition on the deformation and fracture behavior of a precipitation-hardened nickel-base superalloy, Acta Mater. 186 (2020) 616–630.
[19] I. Khan, V. Bhasin, On the role of secondary voids and their distribution in the mechanism of void growth and coalescence in porous plastic solids, Int. J. Solids Struct. 108 (2017) 203–215.
[20] J. Koplik, A. Needleman, Void growth and coalescence in porous plastic solids, Int. J. Solids Struct. 24 (8) (1988) 835–853.
[21] A.C. Lee, A. Parakh, S. Lam, A. Sleugh, O. Tertuliano, D. Doan, J.N. Weker, P. Hosemann, X.W. Gu, Dynamic fracture processes in hydrogen embrittled iron, Acta Mater. 259 (2023) 119234.
[22] A.C. Lee, A. Parakh, A. Sleugh, O.A. Tertuliano, S. Lam, J.N. Weker, P. Hosemann, X.W. Gu, Detection of voids in hydrogen embrittled iron using transmission X-ray microscopy, Int. J. Hydrog. Energy 48 (5) (2023) 1968–1978.
[23] Y. Liang, D.C. Ahn, P. Sofronis, R.H. Dodds, D. Bammann, Effect of hydrogen trapping on void growth and coalescence in metals and alloys, Mech. Mater. 40 (3) (2008) 115–132.
[24] M. Lin, H. Yu, Y. Ding, G. Wang, V. Olden, A. Alvaro, J. He, Z. Zhang, A predictive model unifying hydrogen enhanced plasticity and decohesion, Scr. Mater. 215 (2022) 114707.
[25] M. Marteleur, J. Leclerc, M.S. Colla, V.D. Nguyen, L. Noels, T. Pardoen, Ductile fracture of high strength steels with morphological anisotropy, Part I: characterization, testing, and void nucleation law, Eng. Fract. Mech. 244 (2021) 107569.
[26] T. Matsuo, J. Yamabe, S. Matsuoka, Effects of hydrogen on tensile properties and fracture surface morphologies of Type 316L stainless steel, Int. J. Hydrog. Energy 39 (7) (2014) 3542–3551.
[27] L. Morin, J.C. Michel, Void coalescence in porous ductile solids containing two populations of cavities, Eur. J. Mech. A/Solids 72 (2018) 341–353.
[28] M. Nagumo, K. Takai, The predominant role of strain-induced vacancies in hydrogen embrittlement of steels: overview, Acta Mater. 165 (2019) 722–733.
[29] M. Nagumo, H. Yoshida, Y. Shimomura, T. Kadokura, Ductile crack growth resistance in hydrogen-charged steels, Mater. Trans. 42 (1) (2001) 132–137.
[30] A. Needleman, V. Tvergaard, An analysis of ductile rupture modes at a crack tip, J. Mech. Phys. Solids 35 (2) (1987) 151–183.
[31] T. Neeraj, R. Srinivasan, J. Li, Hydrogen embrittlement of ferritic steels: observations on deformation microstructure, nanoscale dimples and failure by nanovoiding, Acta Mater. 60 (13) (2012) 5160–5171.
[32] K.L. Nielsen, V. Tvergaard, Failure by void coalescence in metallic materials containing primary and secondary voids subject to intense shearing, Int. J. Solids Struct. 48 (9) (2011) 1255–1267.
[33] P.J. Noell, R.B. Sills, A.A. Benzerga, B.L. Boyce, Void nucleation during ductile rupture of metals: a review, Prog. Mater. Sci. 135 (2023) 101085.
[34] A. Pandolfi, M. Ortiz, Use of effective multiscale cohesive models in the simulation of spall in metal plates, Int. J. Numer. Methods Eng. 125 (9) (2024) e7446.
[35] K. Takai, H. Shoda, H. Suzuki, M. Nagumo, Lattice defects dominating hydrogen-related failure of metals, Acta Mater. 56 (18) (2008) 5158–5167.
[36] Z. Tarzimoghadam, D. Ponge, J. Klöwer, D. Raabe, Hydrogen-assisted failure in Ni-based superalloy 718 studied under *in situ* hydrogen charging: the role of localized deformation in crack propagation, Acta Mater. 128 (2017) 365–374.
[37] C. Tekoglu, Void coalescence in ductile solids containing two populations of voids, Eng. Fract. Mech. 147 (2015) 418–430.
[38] P.F. Thomason, A three-dimensional model for ductile fracture by the growth and coalescence of microvoids, Acta Metall. 33 (6) (1985) 1087–1095.
[39] V. Tvergaard, Interaction of very small voids with larger voids, Int. J. Solids Struct. 35 (30) (1998) 3989–4000.
[40] V. Tvergaard, A. Needleman, Analysis of the cup-cone fracture in a round tensile bar, Acta Metall. 32 (1) (1984) 157–169.

[41] Y. Wang, H. Toda, Y. Xu, K. Shimizu, K. Hirayama, H. Fujihara, A. Takeuchi, M. Uesugi, *In-situ* 3D observation of hydrogen-assisted particle damage behavior in 7075 Al alloy by synchrotron X-ray tomography, Acta Mater. 227 (2022) 117658.
[42] H. Yu, A. Díaz, X. Lu, B. Sun, Y. Ding, M. Koyama, J. He, X. Zhou, A. Oudriss, X. Feaugas, Z. Zhang, Hydrogen embrittlement as a conspicuous material challenge-comprehensive review and future directions, Chem. Rev. 124 (10) (2024) 6271–6392.
[43] H. Yu, J.S. Olsen, J. He, Z. Zhang, Effects of loading path on the fracture loci in a 3D space, Eng. Fract. Mech. 151 (2016) 22–36.
[44] H. Yu, J.S. Olsen, J. He, Z. Zhang, Hydrogen-microvoid interactions at continuum scale, Int. J. Hydrog. Energy 43 (21) (2018) 10104–10128.
[45] Z.L. Zhang, C. Thaulow, J. Ødegård, A complete Gurson model approach for ductile fracture, Eng. Fract. Mech. 67 (2) (2000) 155–168.
[46] L. Zybell, G. Hütter, T. Linse, U. Mühlich, M. Kuna, Size effects in ductile failure of porous materials containing two populations of voids, Eur. J. Mech. A/Solids 45 (2014) 8–19.